Chemical Engineering Journal 162 (2010) 883–892

Contents lists available at ScienceDirect

Chemical Engineering Journal

journal homepage: www.elsevier.com/locate/cej

# Preparation of activated carbons from corncob with large specific surface area by a variety of chemical activators and their application in gas storage

Yong Sun, Paul A. Webley*

*Department of Chemical Engineering, Monash University, Wellington Road, Clayton, VIC 3800, Australia*

ARTICLE INFO

*Article history:*
Received 28 March 2010
Received in revised form 22 June 2010
Accepted 24 June 2010

*Keywords:*
Activated carbon
Corncob
Hydrogen adsorption

ABSTRACT

Activated carbons were produced from agricultural waste corncob using a variety of different activation strategies and activators. The BET specific surface area and pore volume of the carbons produced by a two-step KOH activation process were 3012 $m^2/g$ and 1.7 $cm^3/g$, respectively. All carbons prepared showed a microporous character, except for that prepared by a one-step phosphorous acid activation which exhibited hysteresis of a mesoporous carbon. The hydrogen adsorption performance of the different carbons was closely investigated. The microporous carbon with the largest BET specific surface area showed $H_2$ adsorption capacities up to 2.0 wt% at 77 K under 1 atm pressure and 0.44 wt% at 298 K at 5 MPa. The adsorption isotherm model based on the Langmuir–Freundlich equation together with Soave–Redlich–Kwong equation of state for determination of the gas phase fugacity provided a satisfactory representation of the high pressure hydrogen data. The parameter representing full coverage of the solid surface from the Langmuir–Freundlich equation is 9.73 mmol/g or 2 wt% at 298 K. The carbon with the largest hydrogen uptake capacity still cannot meet the US DOE target for hydrogen storage of 6 wt%. The isosteric heat of adsorption of carbon was 7 kJ/mol, typical of a physisorption character and in agreement with literature for the hydrogen–carbon interaction.



## 1. Introduction

To address the present energy and environmental problems caused by fossil fuels, considerable attention has been paid to the use of hydrogen as an energy carrier due to the fact that it is readily made from renewable sources, burns in a pollution-free manner, and contains a higher chemical energy per unit mass than most hydrocarbon fuels [1]. In spite of these advantages, there are several major technical and social hurdles to overcome before a transition to an economy based on hydrogen can be envisaged. One of the most difficult technical hurdles is the storage of hydrogen. Several approaches have been proposed for hydrogen storage. These include high pressure tanks for gaseous hydrogen storage, cryogenic vessels for liquid hydrogen storage, formation of metal hydrides, chemical storage (such as ammonia borane) and physisorption on a large number of proposed adsorbents.

Among the approaches listed above, physisorption has gained much attention due to its reversible nature, and relatively high storage capacity. Activated carbon is a good candidate because of its well-developed porosity, low density, good chemical stability, ready availability and low cost [2]. However, common carbon adsorbents with specific surface area around 1000–1600 $m^2/g$ still cannot achieve the gravimetric and volumetric hydrogen storage requirements. In the past few years, many attempts have been made to prepare carbons with ultra-high specific surface area either from non-renewable resources such as coal, pitch, etc. [3], or using complex, high energy synthesis technologies such as chemical vapor deposition (CVD) [4].

Preparation of activated carbon with ultra-high specific surface area from biomass such as lignin, corncob, cornstalk, dates, etc., has attracted much attention. Among these carbon sources, corncob is a good precursor for preparing carbon with ultra-high specific surface area [5]. The carbons prepared from corncob have been used in wastewater treatment such as removal of organic pollutants [6]. However, a comprehensive study of activating corncob with different chemical activation strategies to prepare carbon with ultra-high specific surface area and pore volumes, and their subsequent performance in gas storage such as the hydrogen adsorption has not to our knowledge been reported. Therefore, in this study we report the synthesis of ultra-high surface area carbon materials using two preparation strategies: a one-step and a two-step chemical activation procedure using different chemical activators such as KOH, $K_2CO_3$, NaOH, $ZnCl_2$, and $H_3PO_4$. We also report the adsorption capacity of those carbons for hydrogen storage.

* Corresponding author at: Department of Chemical Engineering, Monash University, Clayton Campus, VIC 3800, Australia. Tel.: +61 3 99053445; fax: +61 3 99055686.
*E-mail address:* paul.webley@eng.monash.edu.au (P.A. Webley).

1385-8947/$ – see front matter © 2010 Elsevier B.V. All rights reserved.
doi:10.1016/j.cej.2010.06.031

**Table 1**
Main components and elements of raw corncob source.

| Composition | Content (wt%) |
|---|---|
| Cellulose | 36.3 |
| Hemicellulose | 42.8 |
| Lignin | 9.3 |
| Ash | 0.2 |
| Element of corncob | |
| C | 43.4 |
| H | 5.8 |
| N | 0.6 |
| O (Estimated by difference) | 50.2 |

## 2. Experimental work

### 2.1. Preparation of activated carbon

Corncobs were collected in Clayton, Victoria, Australia (the corn is called *Hybrids Ludan-50*) and ground and sieved to about 0.015–0.30 mm in size after air drying at 110 °C for 6 h in an oven. The elemental analysis of the corncob was conducted by FLASH EA1112 elemental analyzer, and the results are shown in Table 1. The content of hemicellulose and carbon is relatively higher than other compositions. These results suggest that corncob is a good natural precursor for production of activated carbon.

We adopted two different preparation strategies: a two-step activation and a one-step activation procedure. Five different carbons were prepared by these two preparation strategies. The alkali-KOH, $K_2CO_3$, and NaOH were used in the two-step activation procedure. According to the literature, a two-step activation process (first pre-carbonizing the corncob then impregnating the chemical activator-alkali with the pre-carbonized char) can produce carbon with a high specific surface area [7]. The char that was prepared from pre-carbonizing corncob was prepared by the following procedures: the dried meshed corncob was carbonized at 450 °C for 4 h in a nitrogen gas environment. In a typical two-step activation process, 1 g of pre-carbonized char was soaked with KOH, $K_2CO_3$, or NaOH solutions respectively at a concentration of 3 mol/l (24 ml) for 2 h at room temperature. These char containing solutions were then treated with ultrasound for 6 h at room temperature. Afterwards, the chars were separated by filtration and activated at different temperatures for 120 min. After the activation, all the samples were washed with hot distilled water. This was continued until the pH value of the washing effluent reached approximately 7. The wet samples were then dried at 105 °C overnight. All the carbons showed a maximum BET specific surface area when activated at approximately 800 °C. The carbons activated by KOH, $K_2CO_3$, and NaOH with the largest BET specific surface area were denoted as C1, C2, C3, respectively. The pre-carbonized corncob char, which was used to soak with alkali, is denoted as PCC.

In a typical one-step activation process, 2 g corncob was soaked with $H_3PO_4$ 50 wt% (with ratio of 1 by weight) or $ZnCl_2$ (50 g/l 40 ml) respectively for 2 h at room temperature. The corncob was separated by filtration and activated at different temperatures for 120 min. The washing procedure was the same as that described above. The largest BET specific surface of the resultant carbon for $H_3PO_4$ activation was obtained at 500 °C, while the largest area obtained for $ZnCl_2$ activation was achieved at 600 °C. Those two carbons were denoted as C4 and C5, respectively.

### 2.2. Characterization of the activated carbon

A variety of techniques were used to characterize the synthesized carbon materials. These included gas adsorption analysis, TGA analysis, FT-IR analysis, SEM and XRD.

*Gas adsorption analysis*: The specific surface area and porosities of the activated carbon samples were determined by nitrogen gas adsorption–desorption at 77 K with the saturation pressure of 106.65 kPa using an ASAP 2020 Automated Gas Sorption System. The BET surface area was assessed within the range of relative pressures from 0.05 to 0.3. The micropore volume was measured by the DR method [8]. The total pore volume was calculated by measuring the amount of $N_2$ adsorbed at a relative pressure of 0.99. The averaged pore width is calculated based on the BJH method [9]. The relative pressure $Pr_I$ is assumed to be close to the unity so that substantially all the pores in the samples are filled. The corresponding Kelvin core radius is calculated. Only pores smaller than this size will be included:

$$Rc_I = \frac{-A}{(1+F)[\ln(Pr_I)]}$$

where $A$ is adsorbate property factor, and $F$ is fraction of pores open at both ends. The Kelvin radius for the end of interval is calculated as follows:

$$Rc_{K+1} = \frac{-A}{(1+F)[\ln(Pr_{I+1})]}$$

All new pores in this interval are represented by one pore having a length-weighted average diameter and corresponding length sufficient to account for the required volume of adsorbate. The weighted average pore diameter is calculated as follows:

$$D_{avg} = \frac{(2)(Rc_K + Rc_{K+1})(Rc_K)(Rc_{K+1})}{Rc_K^2 + Rc_{K+1}^2}$$

The DFT method (by using slit shaped geometry) was used for the pore size distribution of the resulting carbons in the micropore and mesopore range. In the system of carbon adsorbents and nitrogen, the nitrogen–nitrogen interaction is modeled by a Lennard–Jones pairwise interaction potential:

$$U_{NN}(r) = 4\varepsilon_{NN}\left[\left(\frac{\sigma_{NN}}{r}\right)^{12} - \left(\frac{\sigma_{NN}}{r}\right)^{6}\right]$$

where $r$ is the internuclear separation of molecules, $\varepsilon_{NN}$ is the depth of inter-molecular potential well, and $\sigma_{NN}$ is molecular diameter. The resultant carbon–nitrogen interaction potential for a slit-like pore is given by:

$$U_{CN}(Z)\left\{\begin{array}{l} = U(Z) + U_1(w - Z);\ 0 < Z < w \\ = \infty;\ \text{otherwise} \end{array}\right\}$$

$$U_1(Z) = 2\pi\varepsilon_{CN}\sigma_{CN}^2\rho_c\Delta\left[0.4\left(\frac{\sigma_{CN}}{Z}\right)^{10} - \left(\frac{\sigma_{CN}}{Z}\right)^{4} - \frac{\sigma_{CN}^4}{3\Delta(Z+0.61\Delta)^3}\right]$$

where $\varepsilon_{CN}$ and $\sigma_{CN}$ are the energy and size parameters of carbon–nitrogen interaction, $\rho_c$ ($\rho_c = 114\,\text{nm}^{-3}$) is the number density of carbon atoms in graphite, and $\Delta$ ($\Delta = 0.335$ nm) is the separation of graphite planes. The total adsorption on a porous carbon can be expressed by:

$$N(p) = \int_{H\,\min}^{H\,\max} f(H)\rho(H,p)dH$$

where $N(p)$ denotes the volume adsorbed as function of pressure, $H_{\min}$ and $H_{\max}$ are widths of the smallest and largest pores present and $\rho(H,p)$ is molar density of nitrogen at pressure p in a pore width H. The pore size distribution, $f(H)$ is the distribution of pore volumes as function of pore width. In this approach, the individual pore model for nitrogen adsorption is on the basis of nonlocal density approximation. The DFT pore size distribution is based on the assumption that the pore size distribution of a sample could be described by a bimodel log-normal distribution function, the six

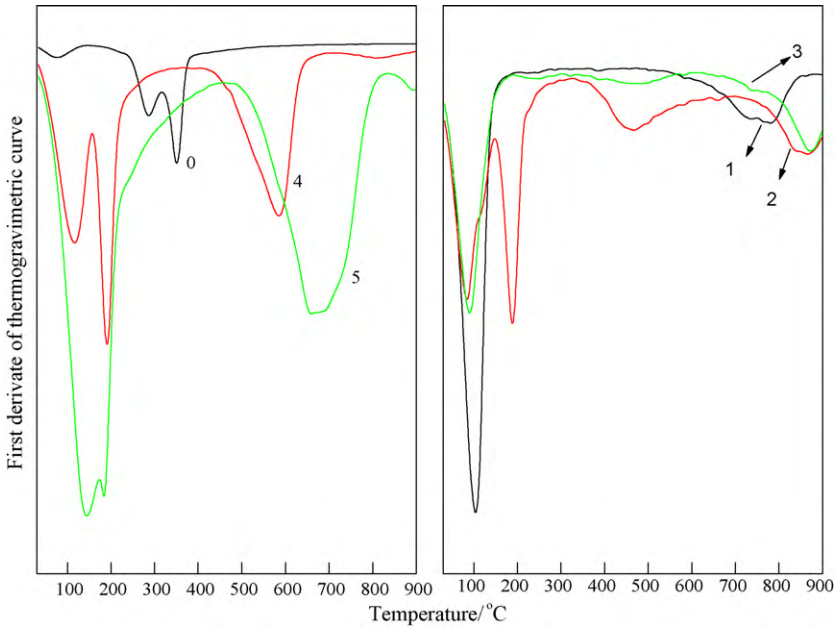


**Fig. 1.** Thermal behavior of different carbons under $N_2$ atmosphere during pyrolysis where (0) corncob, (1) PCC+KOH, (2) PCC+$K_2CO_3$, (3) PCC+NaOH, (4) Corncob+$ZnCl_2$, (5) Corncob+$H_3PO_4$.

parameters of the distribution were determined by a multilinear least square fitting of parameterized computed model isotherms to data. In this study, the pore size distribution was calculated using DFT software provided by the Micromeritics Instrument Corporation.

*TGA analysis*: Thermal gravimetric analysis was conducted by TGA/SDTA851 by pyrolysis of the sample up to 900 °C in the presence of nitrogen.

*FT-IR analysis*: The Spectrum GX (Perkin-Elmer USA 2003) infrared spectrometer was used for the study of the surface functional groups. Discs were prepared by mixing the 0.5 mg sample with 200 mg of KBr (Merck, for spectroscopy) in an agate mortar and then pressing the result mixture at 2 MPa for 1 min. The samples were scanned in the spectra range of 4000–370 $cm^{-1}$.

*X-ray diffraction (XRD) analysis*: XRD patterns were obtained with a Philips X'pert diffractometer using Cu Kα radiation at a wavelength of λ = 1.5406 Å. A thin powder sample was placed onto an oriented monocrystalline quartz plate and scanned from 10 to 90°.

*Surface morphology*: Surface morphology was examined using a HITACHI S-450 scanning electron microscope.

### 2.3. Gas adsorption measurements

*Low pressure and cryogenic hydrogen adsorption*: Hydrogen adsorption characterization was determined by hydrogen gas adsorption at 77 K using a ASAP 2010 Automated Gas Adsorption Analyzer System. Before the test, all the samples were degassed ($10^{-6}$ Torr) at 350 °C over night in order to pass the leak test of the ASAP 2010. The hydrogen used in this experiment was high purity grade (99.999%) supplied by Linder Gas.

*Hydrogen high pressure adsorption*: Hydrogen adsorption up to 5 MPa was also conducted on sample C1. The high pressure adsorption measurement was performed on a magnetic suspension balance (Rubotherm, Bochum Germany). For the measurement, approximate 1 g of sample was used after degassing at 573 K for 24 h. The hydrogen was introduced to the desired pressure and when thermodynamic equilibrium was reached, the amount of adsorbed gas was calculated by balance reading. At each point, the sample weight was measured three times and averages taken. The hydrogen used in this experiment was high purity grade (99.9999%) supplied by Coregas.

## 3. Results and discussion

### 3.1. TGA analysis

Thermograms obtained from the thermogravimetric analysis of corncob as well as the carbons activated with different chemical activators are shown in Fig. 1. The weight loss during the TG analysis of corncob is divided into three stages. The first stage occurs around 100 °C, which corresponds to elimination of loosely bound moisture. The second stage occurs around 250 °C, which corresponds to elimination of fixed water. The third stage occurs at around 350 °C, which relates to elimination of the material such as cellulose, hemicellulose and lignin [10]. The pyrolysis behavior of the carbons produced from the corncob activated with $ZnCl_2$ and $H_3PO_4$-so called one-step activation, are different to that of the carbons that are produced PCC prepared with two-step activation, in terms of the temperature at which maximum weight loss occurs.

In the case of the one-step preparation procedure, the TGA also exhibits three stages. The first and second stages are around 100 and 200 °C, respectively, which are due to the elimination of moisture and fixed water of the carbons. The third stage occurs around 600 °C for $ZnCl_2$ activation and 700 °C for $H_3PO_4$ activation, respectively. Comparing the TG analysis of the effect of temperature upon BET specific surface area of the produced carbons, we find that carbon activated by $ZnCl_2$ reaches its maximum BET specific surface area when activation temperature reaches 600 °C, which is also the temperature at which the corncob + $ZnCl_2$ experiences its maximum weight loss in its third stage. However, the carbon produced from $H_3PO_4$ activation reaches its maximum BET specific surface area only at 600 °C, which is lower than its maximum weight loss temperature at the third stage. This indicates that the maximum weight loss does not necessarily correspond to its optimal condition in producing carbon with the largest BET specific surface area and pore volume.

In case of the carbon produced from the two-step preparation procedure, all carbons activated by alkali-KOH, $K_2CO_3$, NaOH

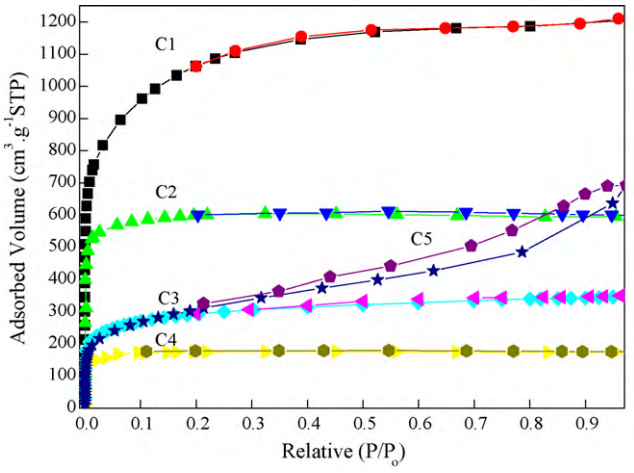


**Fig. 2.** Adsorption–desorption isotherms of different carbons.

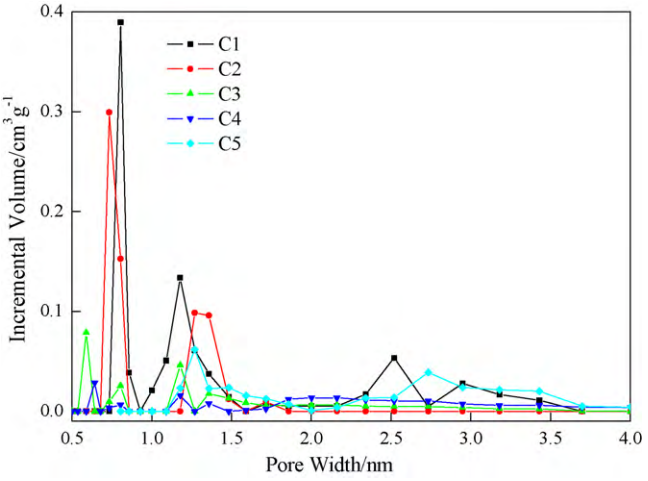


**Fig. 3.** DFT pore size distribution of different carbons.

show their major weight loss in the temperature range from 800 to 850 °C, which corresponds to the optimal preparation conditions for producing carbon with the largest BET specific surface area and pore volume. This is due to the fact that the reaction between the carbon and alkali around 850 °C facilitates pore formation and pore development of the carbon skeleton [6].

The TG analysis indicates that the optimal preparation conditions with the largest BET specific surface area and pore volume generally corresponds to the maximum weight loss rate at certain temperature ranges in the case of the carbon activated by $ZnCl_2$, and alkali-KOH, $K_2CO_3$, NaOH, respectively. The only exception is the case of $H_3PO_4$ activation, in which the optimal preparation temperature for producing carbon with the largest BET specific surface area and pore volume is lower than its corresponding maximum weight loss temperature.

### 3.2. Characterization of resulting carbons

After chemical activation, we selected the carbons with the largest BET specific surface area and pore volume from those five different activation approaches and performed further analysis. These are samples C1, C2, C3, C4, C5, respectively.

#### 3.2.1. Nitrogen adsorption/desorption

The nitrogen adsorption isotherms of different carbons are shown in Fig. 2. According to Brunauer–Deming–Deming–Teller (BDDT) classification [11], C1, C2, C3, C4 all exhibit the typical type I isotherm. The major uptake occurs at a relatively low pressure, indicating the formation of highly microporous materials with a narrow pore size distribution, these materials are essentially entirely microporous. On the other hand, C5 exhibits the type IV isotherm. The hysteresis effect and slope of plateau with significant increase in the nitrogen uptake through the entire pressure range indicates the presence of mesopores. Fig. 3 shows the micropore distribution of different carbons by the DFT method. The carbons activated by KOH and $K_2CO_3$ (C1, C2), show good pore development in the microporous region, while the other carbons have relatively poor pore development in this region. A large proportion of micropores of C1 and C2 distribute in the range of 0.5–1.3 nm. In the case of C5, pore development occurs in the microporous and mesoporous region (>20 Å). The porosity parameters obtaining from $N_2$ adsorption isotherm of different carbons are summarized in Table 2. By comparing the parameters, it is clear that the two-step KOH activation with the aid of ultrasonic treatment during the infiltration process can produce carbon with ultra-high BET specific surface area (3012 m$^2$/g) and pore volume (1.7 cm$^3$/g), respectively. In addition, in case of microporous area, which is by means of t-plot method, the results show that C1 has the highest micropore surface area, while C5 has the smallest one. This indicates good micropore development in C1 and relative poor micropore development in C5. In the case of average pore width of different carbons, carbon C4, which is prepared by the one-step activation by $ZnCl_2$, has the smallest average pore width, which is equal to 1.75 nm. The carbon C5 has the largest average pore width of 4.01 nm, which is prepared by a one-step $H_3PO_4$ activation.

The comparison between our work and other literature concerning with preparation conditions of activated carbon with ultra-high specific surface area from corncob is shown in Table 3. It can be seen that KOH is more effective than other activators such as $K_2CO_3$, $CO_2$ in activating the corncob. In addition, the activation procedure is also important to the development of micropores. The BET specific surface area of the carbon from one-step activation, in which the corncob is directly impregnated with KOH, was approximately 2000 m$^2$/g, while the BET specific surface area of the carbon produced by the two-step activation procedure, in which the corncob is firstly pre-carbonized and then the carbonized char is impregnated with KOH, was approximately 3000 m$^2$/g. Moreover, the infiltration step is an important factor to the development of micropores. After the ultrasonic treatment during infiltration, the chemical activator

**Table 2**
Total pore volumes, micropore volume, BET specific surface areas, micropore areas, and average pore widths of different carbons.

| Sample | Pore volume (cm$^3$/g) | Micropore volume (cm$^3$/g) | BET specific surface area (m$^2$/g) | Micropore area (m$^2$/g) | External surface area (m$^2$/g) | Average pore width (nm) |
|---|---|---|---|---|---|---|
| PCC | 0.1 | 0.06 | 160 | 130 | 30 | 1.83 |
| C1 | 1.7 | 0.98 | 3012 | 2118 | 894 | 2.28 |
| C2 | 0.9 | 0.77 | 2080 | 1729 | 351 | 1.76 |
| C3 | 0.5 | 0.26 | 1006 | 581 | 425 | 2.05 |
| C4 | 0.3 | 0.24 | 606 | 546 | 67 | 1.75 |
| C5 | 1.0 | 0.10 | 1069 | 168 | 901 | 4.01 |

**Table 3**
Comparison of preparation conditions and the main parameters of different carbons with large specific surface area from corncob.

| Preparation Condition | BET specific surface area ($m^2/g$) | Pore Volume ($cm^3/g$) | Reference |
|---|---|---|---|
| Carbonization at 450 °C for 2 h, char impregnating with KOH with ultrasonic treatment then activated at 850 °C | 3012 | 1.7 | This work |
| Carbonization at 350 °C for 5 min, char activation by KOH at 800 °C | 2880 | 1.6 | [5] |
| Carbonization at 450 °C for 1.5 h, char activation with KOH at 780 °C plus $CO_2$ gasification | 2844 | 1.5 | [12] |
| Carbonization at 450 °C for 1.5 h, char activation with KOH at 780 °C. | 2595 | 1.4 | [13] |
| Carbonization at 450 °C for 2 h, char impregnating with $K_2CO_3$ with ultrasonic treatment then activated at 850 °C | 2112 | 1.0 | This work |
| One-step KOH activation at 800 °C | 1975 | 0.9 | [5] |
| One-step KOH activation at 800 °C plus $CO_2$ gasification | 1806 | 0.8 | [14] |

**Table 4**
Nanographitic structure of the produced carbons.

| Sample | $d_{002}$(nm) | $L_c$(nm) |
|---|---|---|
| 1 | 0.3468 | 1.04 |
| 2 | 0.3482 | 1.06 |
| 3 | 0.3450 | 1.02 |
| 4 | 0.3564 | 1.21 |
| 5 | 0.3542 | 1.38 |

could further enter the inner skeleton of the pre-carbonized corncob, and this complete mixing could facilitate the reaction between the chemical activator and carbon during the activation step. This might be the reason why the carbon prepared from our process produces larger BET specific surface area compared to carbons from other literature. It is clear that the two-step activation with aid of ultrasonic treatment during infiltration produces a carbon with large BET specific surface area. Our reported value of 3012 $m^2/g$ is the maximum reported to date for carbons produced from corncob.

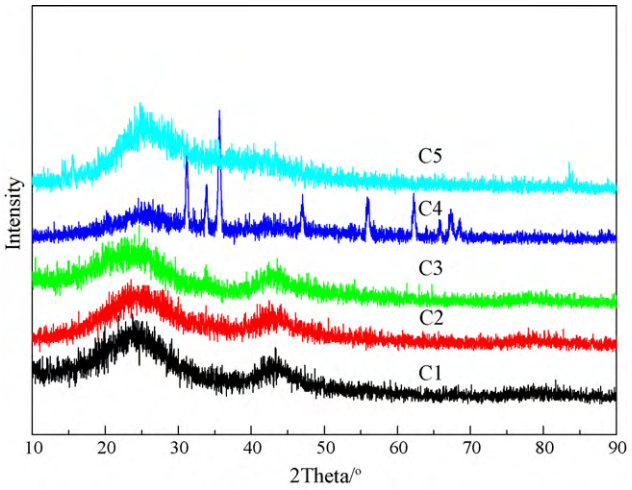


**Fig. 4.** XRD patterns of different carbons.

### 3.2.2. XRD analysis

The carbons produced from corncob with different activators can be crystallographically characterized by means of X-ray diffraction. The interlayer spacing $d_{002}$ and the crystallite size $L_c$ (as determined by Scherrer equation) are given in Table 4. It is seen that carbons activated at relatively higher temperatures of around 800 °C yield relatively smaller values of $d_{002}$ and $L_c$ than carbons that are activated around 600 °C, this phenomena agrees with the literature reports on the carbon produced from jackfruit [15]. The $d_{002}$ and $L_c$ value become slightly smaller as the surface area increases, this was due to the material structural ordering [16]. The $d_{002}$ value, which is listed in Table 4, is in the range of 0.34–0.35. These values are larger than that of graphite (0.335 nm). From Fig. 4,

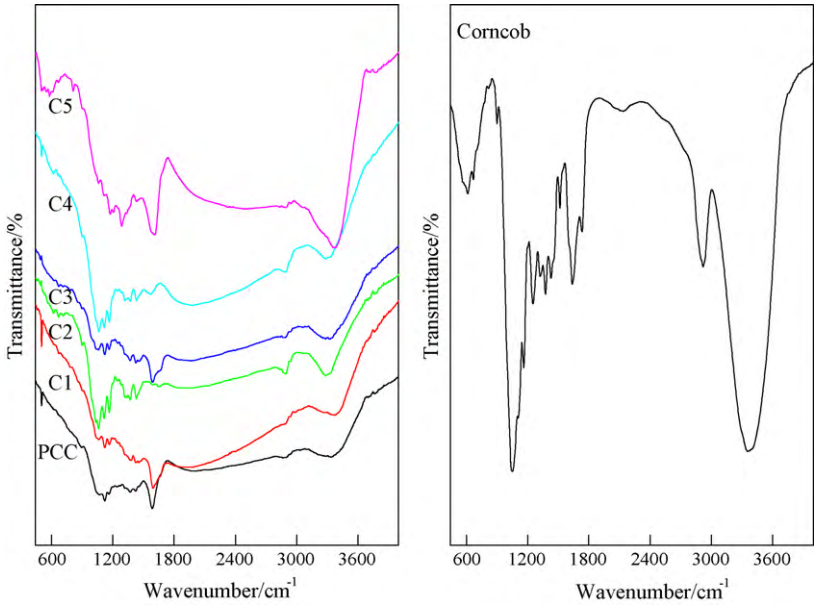


**Fig. 5.** FT-IR spectroscopy of corncob and different carbons.

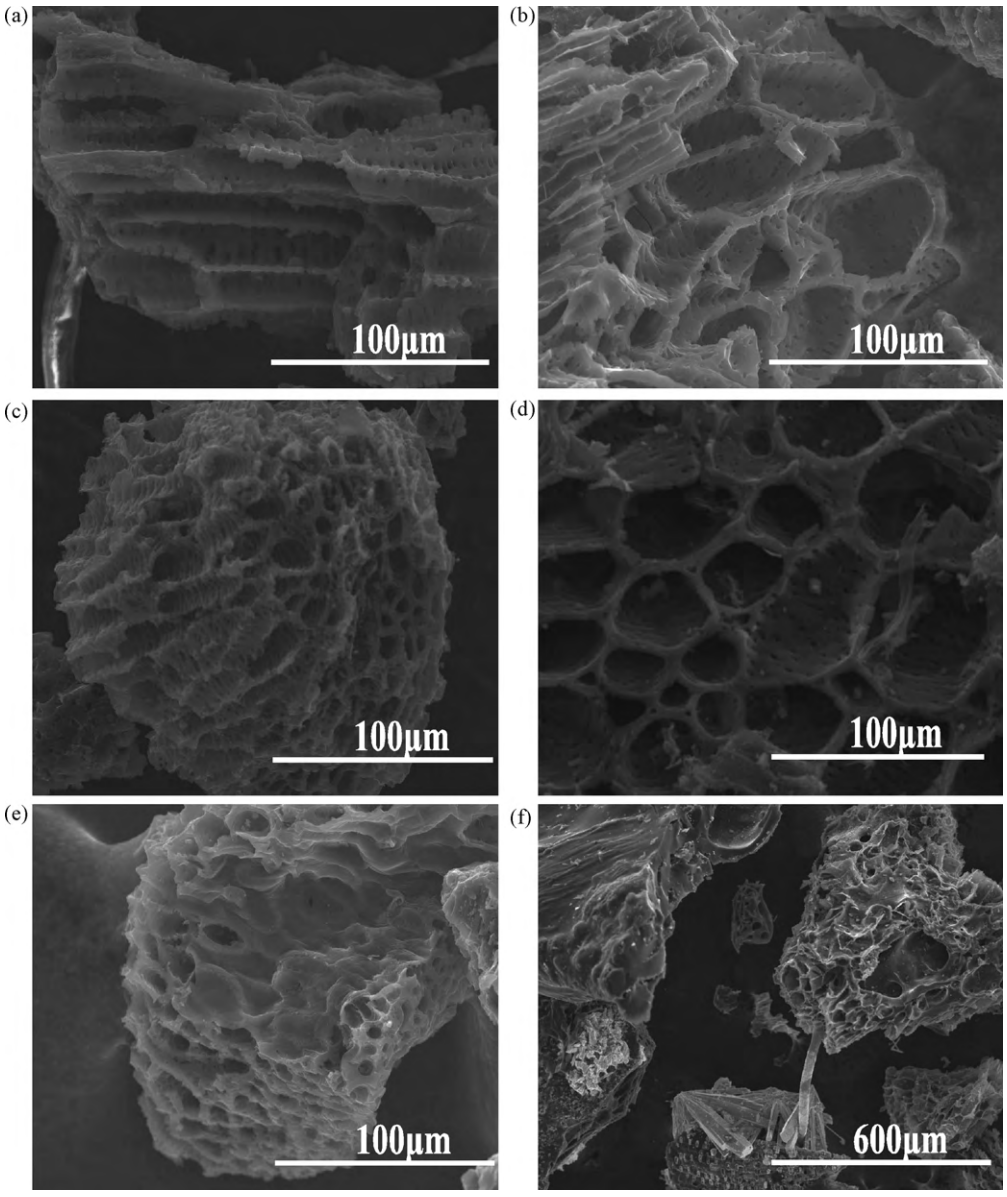


**Fig. 6.** Scanning Electron Microscopy of different carbons, where a, b, c, d, e, f represents PCC, C1, C2, C3, C4, C5, respectively.

most carbons exhibit broad small peaks, centered around 26° and 44°, respectively. For these activated carbons, the broad peaks are assigned to the reflection from graphite (0 0 2) and (1 0) planes, respectively. In addition, in the case of carbon C4, which exhibits certain sharp peaks, the existence of those sharp peaks may be attributed to the existence of residual ash such as zinc in the carbon.

### 3.2.3. FT-IR analysis

The FT-IR spectroscopy of corncob and different carbons is shown in Fig. 5. Before activation, the spectra of corncob presents bands at 1630, 1040, 898 $cm^{-1}$, which are the characteristic adsorption peaks of cellulose, and hemicellulose. In addition, bands at 1600, 1510, 1420, 835 $cm^{-1}$ are characteristic of the aromatic skeleton of lignin macromolecules like p-coumaryl, coniferyl and sinapyl units, which is typical of HGS grass lignin [17]. After carbonization and activation, the intensity of those bands decreased, and even disappeared in some carbons. This is due to the pyrolysis of the corncob during the precarbonization and activation process. All the carbons show the wide band at about 3488–3100 $cm^{-1}$, which is assigned to O–H stretching mode of hexagonal groups and adsorbed water. The band at 2920 $cm^{-1}$, which is assigned to the asymmetric C–H band representing the alkyl groups such as methyl and methylene groups, is observed in all the carbons with different intensity. The variance in intensity of different carbons is due to different activation process, which leads to a different rate of $CH_3$ groups being removed from the substituted aromatic rings during the pyrolysis. The band around 1610 $cm^{-1}$, which is attributed to C=O stretching vibrations of carbonyl groups, is observed in all the carbons with different intensity. All the carbons also show the band around 1180 $cm^{-1}$, which is attributed to C–O stretching vibrations of carbonyl groups. The FT-IR spectroscopy result indicates that the produced carbons are rich in surface functional groups.

### 3.2.4. SEM morphology

The morphology of different carbons is shown in Fig. 6. All the carbons are porous with honeycomb shape, and irregular holes. In addition, from the morphology of PCC, it is seen that when corncob is carbonized, it forms a tubular like channel structure, of 20 μm in diameter and 100 μm in length. The carbon samples C1, C2, C3, C4, C5 all retain a similar morphology to PCC, but with differ-

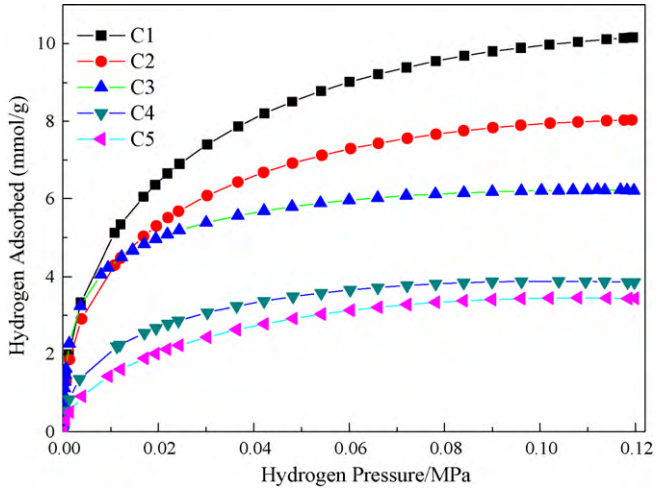


**Fig. 7.** Adsorption isotherm of hydrogen at 77 K on different carbons.

ent pore sizes. The pore width of C1 is from 10 to 100 μm, C2 is around 10 μm, C3 is around 30 μm, C4 is 10 μm, and C5 is around 40 μm. It can be inferred that the existence of these macropores facilitates soaking of activator such as KOH during the infiltration process, which facilitates the reaction between chemical activator and the carbon skeleton during the activation process, and this in turn results in a good pore development, especially for C1, which has the largest micropore surface area and pore volume.

### 3.3. Gas adsorption

One of the most important applications of the carbons with good microporous development is in the field of gas storage. In this work, we tested different carbons for their hydrogen storage capacity.

#### 3.3.1. Hydrogen adsorption under 1 atm and 77 K

The adsorption isotherms of different carbons in adsorbing hydrogen at 77 K under 1 atm are shown in Fig. 7. The hydrogen adsorbed on C1 is higher than that of other carbons and up to 2 wt% $H_2$ is adsorbed at 1 atm at 77 K. Although the nitrogen adsorption data shows that C5 can adsorb more nitrogen at the high relative pressure range than C3 and C4, the hydrogen adsorption capacity of C5 at cryogenic condition is inferior since it has a very low micropore area and volume. This result also agrees with the literature reports [4]. The relationship between hydrogen adsorption capacities and micropore volume and micropore specific surface area is shown in Fig. 8. The result indicates that there is an approximate linear relationship between the hydrogen adsorption capacity and micropore volumes as well as the micropore specific surface area. This result agrees with the report that micropores play the most important role in hydrogen uptake [4]. It is interesting to note that although the difference of micropore volumes of C3 and C4 is not large, their hydrogen adsorption performance is very different. This difference might be due to ash contents remaining in the prepared samples, or different functional groups on C3 and C4, or even the numbers of ultra-micropores in these two samples, which could not be detected by the $N_2$ adsorption isotherm data. Further work is needed to understand these effects.

#### 3.3.2. Hydrogen adsorption under high pressure at room temperature

In addition to testing the capacity of the resultant carbons in adsorbing hydrogen at cryogenic condition, we also tested the capacity of C1 in adsorbing hydrogen at high pressure at room temperature. We adopted the Soave–Redlich–Kwong (SRK) equation to determine fugacity and compressibility factor for hydrogen:

$$\ln\frac{f}{P} = z - 1 - \ln(z - B^*) - \frac{A^*}{B^*}\ln\left(1 + \frac{B^*}{z}\right)\alpha \tag{1}$$

where $f$ is fugacity, $z$ is the compressibility factor. $A^*$ and $B^*$ can be determined from three parameters of the gas: critical pressure $Pc$; critical temperature $Tc$ and the eccentric factor $\omega$:

$$A^* = 0.4278 \cdot z \cdot \frac{P/Pc}{(T/Tc)^2} \tag{1a}$$

$$B^* = 0.0867 \cdot \frac{P/Pc}{(T/Tc)} \tag{1b}$$

$$\alpha^{0.5} = 1 + m(1 - Tr^{0.5}) \tag{1c}$$

$$m = 0.480 + 1.574\omega - 0.176\omega^2 \tag{1d}$$

The parameters of hydrogen are $\omega = -0.216$, $m = 0.131805$, $\alpha = 0.5429$, respectively. From the experimental data of pressure to determine fugacity and gas density at the experimental temperature, then using Langmuir–Freundlich equation to yield the relevant constants in this equation:

$$n^{\Omega} = n_m^*\left(\frac{bP^q}{1 + bP^q}\right) = n + v_a\rho_g \tag{2}$$

where the $n^{\Omega}$ is the absolute adsorption mmol/g, $n$ is the excess adsorption obtained from the measurement (mmol/g), $n_m^*$ is a parameter that corresponds to full coverage of solid surface, $v_a$ is the volume of adsorbate in the adsorbed phase $m^3/g$, $\rho_g$ is the density of the bulk gas $mol/m^3$, b and q are the parameters of the Langmuir–Freundlich equation. By using the assumption of monolayer arrangement of adsorbate molecules adsorbed above the critical temperature, the following relation holds:

$$v_a = \theta S\sigma_{sg} \tag{3}$$

where $\theta$ is the percentage of the surface when the adsorbed amount is $n$; $S$ is the specific surface area of the adsorbent, $m^2/g$; and $\sigma_{sg}$ is the depth of the adsorbed layer, $m$. The subscript "$sg$" denotes the interaction between solid and gas. Since $\theta = n^{\Omega}/n_m^*$, it holds Eq. (3) that

$$v_a = \left(\frac{bP^q}{1 + bP^q}\right)S\sigma_{sg} \tag{4}$$

The quantity $\sigma_{sg}$ is an "average reach" of an adsorbed molecule, and is related to $n_m^*$ by:

$$S = n_m^* A_v \sigma_{sg}^2 \tag{5}$$

where is $A_v$ is the Avogadro number.

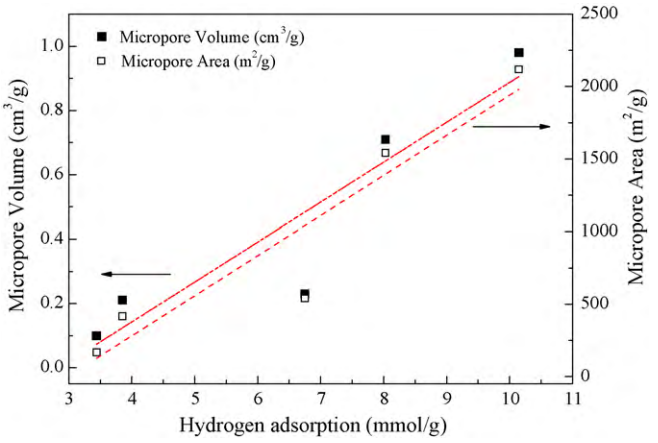


**Fig. 8.** The relationship between hydrogen adsorption capacities (at 77 K and 1 bar) and micropore volume and micropore surface area.

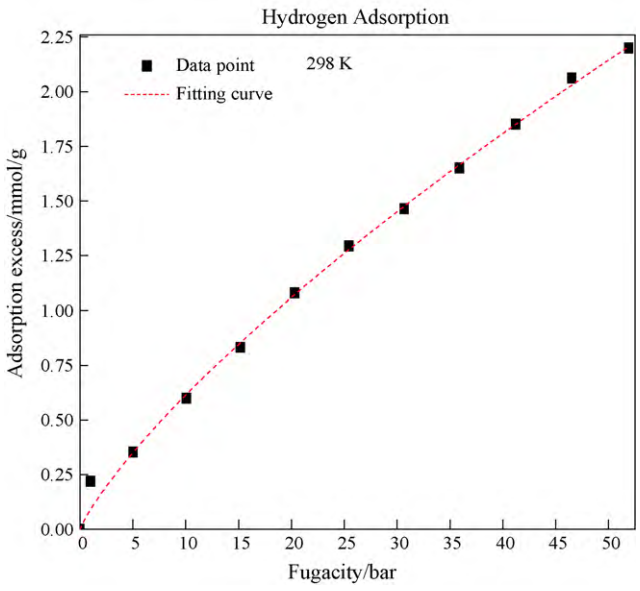


**Fig. 9.** Adsorption data of hydrogen at 298 K up to 5 MPa on C1.

By substituting Eqs. (3)–(5) into Eq. (2), we obtain

$$n = \left(\frac{bP^q}{1+bP^q}\right)\left(n_m^* - \frac{S^{3/2}}{(n_m^* A_v)^{1/2}}\rho_g\right) \tag{6}$$

Then pressure $P$ should be replaced by fugacity at high pressure. The Eq. (6) is therefore modified to Eq. (7):

$$n = \left(\frac{bf^q}{1+bf^q}\right)\left(n_m^* - \frac{S^{3/2}}{(n_m^* A_v)^{1/2}}\rho_g\right) \tag{7}$$

By fitting the excess adsorption data of C1 into Eq. (7), we obtained the constants $b$ $q$ $n_m^*$, respectively. The non-linear curving fitting result is shown in Fig. 9. The constants from fitting the non-linear equation of $b, q, n_m^*$ are 0.0079, 0.9191, 9.7294 (mmol/g), respectively. The relative variance $r^2$ is over 0.999. The adsorption isotherm model up to 5 MPa at 298 K for hydrogen adsorption thus is obtained as following:

$$n = \left(\frac{0.0079f^{0.9191}}{1+0.0079f^{0.9191}}\right)(9.7294 - 0.6819\rho_g) \tag{8}$$

The value of $n_m^*$ indicates that the sample C1 can reach 9.7294 (mmol/g) at 298 K, which is almost 1.95 wt%, when the full coverage of solid surface by hydrogen on C1 is reached. However, based on our experimental conditions, which is 5 MPa and 298 K, the hydrogen adsorption capacity of C1 is only about 0.44 wt%. This adsorption capacity is still far below the US Department of Energy target of 6.5 wt% at room temperature.

The hydrogen adsorption capacity by different carbon adsorbents under different adsorption conditions is compared in Table 5. The maximum hydrogen adsorption capacity of C1 is 2.0 wt% at 77 K at 1 atm and 0.44 wt% at 298 K and 5 MPa, which is comparable to the literature reports. By comparison from Table 5, in terms of physisorption, the hydrogen uptake generally agrees with the development of pores, especially development of micropores, such as the BET specific surface area, micropore volumes, etc. With increase of the surface area from 467 $m^2/g$ (reference 26) to 3190 (reference 27), hydrogen adsorption capacity increases from 0.7 to 2.5% (77 K and 1 bar). In addition, as shown in Fig. 3, the pore size of the carbon with ultra-high specific surface area and good hydrogen adsorption performance generally falls into the microporous region, which is between 0.2 and 2 nm. There are some exceptions such as in Ref. [18], in which the hydrogen adsorption performance of the Norit carbon with specific surface area around 200 $m^2/g$ is 1.6 wt% at 77 K 1 bar, which is comparable to that of the carbon with ultra-high specific surface area carbon (3000 $m^2/g$). This discrepancy might be due to the different surface functional groups on the prepared carbons, different characterization methods, and even the purity of the hydrogen gas that was used for the experiment. In terms of chemisorption of hydrogen on the carbons, the adsorbents such as the carbon nanotubes or the carbons loaded with the trace metals often tend to adsorb fairly large amounts of hydrogen even with relatively low specific surface area. But problems of reversibility and regeneration still remain when comparing with physisorption systems. The hydrogen adsorption capacity of metal organic frameworks (MOFs) is very high, reaching 2.0 wt% at 298 K 5 MPa in reference 28, which indicates its advantage and prospects in hydrogen storage.

### 3.3.3. *Isosteric heat of adsorption of hydrogen on activated carbon*

The calculation of the adsorption properties is based on the thermodynamic formalism of Myers and Monson for solute adsorption [29]. The solution thermodynamics is applied to the condensed phase (adsorbent + adsorbed gas). The assumption of constant adsorption volume $V_a$ is essential to the validity of this procedure [30]. The adsorbent is assumed to be rigid and its mass to be fixed. The internal energy $U_c$, the Helmholtz free energy $F_c$ and the grand potential $\Omega_c$ of the condensed phase are given by:

$$U_c = TS_c - PV + \mu n^{\Omega} + \mu_s \tag{9}$$

$$F_c = U_c - TS_c = -PV + \mu n^{\Omega} + \mu_s \tag{10}$$

$$\Omega_c = -PV + \mu_s \tag{11}$$

where $\mu$ is the chemical potential of the equilibrium bulk gas (J/mol), the $\mu_s$ is the chemical potential of the adsorbent (J/kg), $V$ is volume of the condensed phase (constant) ($m^3$/kg). For simplicity, we omit the detailed process of derivation of the formula for differential energy adsorption $\Delta\bar{\mu}_a$ and isosteric heat of adsorption $\Delta\bar{h}_a$, the detailed reproduction of the formula could be found in Richard's et al. [31] work. The differential energy adsorption $\Delta\bar{\mu}_a$ and isosteric heat of adsorption $\Delta\bar{h}_a$ can be expressed as following:

$$\Delta\bar{\mu}_a = \left[\frac{\partial \Delta U_a}{\partial n_a}\right]_{T,V} - \mu_g^0 \tag{12}$$

$$\Delta\bar{h}_a = \Delta\bar{\mu}_a - RT \tag{13}$$

The thermodynamic variables in Eqs. (12) and (13) are calculated using Dubinin–Astakhov (D–A) micropore volume-filling adsorption model based fit, which are frequently used by different authors for high pressure hydrogen adsorption [32,33]. Using the D–A model, the absolute adsorption is:

$$n^{\Omega} = n_{\max} \exp\left[-\left[\frac{RT}{\alpha+\beta T}\right]^m \ln^m\left(\frac{P_0}{f}\right)\right] \tag{14}$$

where $m = 2$ is setting for the carbon hydrogen system and is found to be appropriate, and $n_{\max}$, $\alpha$, $\beta$, $P_0$ needed to be determined for the supercritical region. We then use our C1 hydrogen high pressure adsorption data to yield those four constants by assuming the adsorption volume $V_\alpha$ (0.0015) to be constant. The constants from fitting the D–A equation of $n_{\max}$, $\alpha$, $\beta$, $P_0$ are 6.5, 4300, 19, 1980, respectively. The relative variance $r^2$ is over 0.988. Then the partial differential of $n^{\Omega}$ with respect to $T$ and $f$ are:

$$\left(\frac{\partial n^{\Omega}}{\partial T}\right)_{f,V} = \frac{2\alpha n^{\Omega}\ln(n^{\Omega}/n_{\max})}{T(\alpha+\beta T)} \tag{15}$$

**Table 5**
Comparison of hydrogen adsorption capability of different adsorbent with large specific surface area. BET specific surface area is denoted as SSA; Single-wall carbon nano tube is denoted as SWNTs. Activated carbon is denoted as AC. CMK3 that is activated by $CO_2$ is denoted by CMK3, metal phosphorous molecular sieve is denoted as MPS. CB850 h represents carbon produced by chemical vapor deposition using zeolite $\beta$ as template. Norit, MAXSORB and AX-21 are commercial activated carbons. AC-3NA-373 is activated carbon produced from litchi wood and then was immersed with 100 ml $HNO_3$ (3 N) for 24 h at 373 K. AC-K5 is the carbon activated by KOH with impregnate ratio of 5 and activating at 1023 K. IRMOF-8/Pt/AC is metal-organic frameworks constructed by linking tetrahedral $[Zn4O]^{6+}$ clusters with linear carboxylates, and then impregnating with Pt (5%)/AC with impregnate ratio of 9:1.

| Sample | SSA ($m^2$/g) | $V_{micro}$ ($cm^3$/g) | $H_2$ adsorption at 1 atm 77 K wt% | $H_2$ adsorption at 50 atm 298 K wt% | Reference |
|---|---|---|---|---|---|
| Norit | 164 | 0.07 | 1.6 | 0.25 | [18] |
| SWNTs | 262 | 0.05 | 0.01 | 0.15 | [18] |
| MAXSORB:Pd 1:2 | 199 | 0.06 | 0.52 | 0.30 | [19] |
| AC | 2136 | 1.03 | 2.0 | – | [20] |
| CMK3 | 2749 | 0.96 | 2.27 | – | [21] |
| MPS | – | – | 1.42 | – | [22] |
| A-CMC | 2700 | 1.00 | – | 0.4 | [23] |
| CB850h | 3150 | 1.13 | 2.5 | – | [24] |
| AX-21 | 3000 | – | – | 0.4 | [25] |
| AC | 2623 | 0.72 | 2.5 | – | [26] |
| AC-3NA-373 | 468 | 0.28 | 0.7 | 0.05[a] | [26] |
| AC-K5 | 3190 | 1.1 | 2.5 | – | [27] |
| IRMOF-8/Pt/AC | 466 | – | – | 2.0 | [28] |
| C1 | 3012 | 0.98 | 2.0 | 0.44 | This work |

[a] The high pressure hydrogen adsorption is conducted at 303 K with 5 MPa.

$$\left(\frac{\partial n^{\Omega}}{\partial f}\right)_{T,V} = \frac{2\alpha n^{\Omega} RT\sqrt{-\ln(n^{\Omega}/n_{max})}}{f(\alpha+\beta T)} \quad (16)$$

Using Eq. (14), the fugacity is given by:

$$f = P_0 \exp\left[-\left[\frac{\alpha+\beta T}{RT}\right]\sqrt{-\ln\left(\frac{n^{\Omega}}{n_{max}}\right)}\right] \quad (17)$$

The internal energy of the adsorbed gas relative to the energy of the perfect gas state at 1 atm and the same temperature $\Delta U_a$ can be expressed as following:

$$\Delta U_a = U_a - n^{\Omega}u_g^0 = -\frac{n_{max}(\alpha+\beta T)\sqrt{\pi}}{2}\left[1 - Erf\left(\sqrt{-\ln\frac{n^{\Omega}}{n_{max}}}\right)\right] + n^{\Omega}\left[RT - \alpha\sqrt{-\ln\frac{n^{\Omega}}{n_{max}}}\right] \quad (18)$$

where *Erf* is the error function, here we adopt the following approximation for *Erf*:

$$Erf(x) \approx \sqrt{1 - \exp\left(-x^2 \times \frac{4/\pi + ax^2}{1+ax^2}\right)} \text{ where } a = 0.14 \quad (19)$$

By differentiating Eq. (18), we obtain the partial derivatives with respect to $T$ and $f$:

$$\left(\frac{\partial \Delta U_a}{\partial T}\right)_{f,V} = \frac{2\alpha n^{\Omega}\ln(n^{\Omega}/n_{max})}{T(\alpha+\beta T)} \times \left[RT - \alpha\sqrt{-\ln\left(\frac{n^{\Omega}}{n_{max}}\right)}\right] + n^{\Omega}R \quad (20)$$

$$\left(\frac{\partial \Delta U_a}{\partial f}\right)_{T,V} = \frac{2n^{\Omega}RT}{f(\alpha+\beta T)}\sqrt{-\ln\left(\frac{n^{\Omega}}{n_{max}}\right)} \times \left[RT - \alpha\sqrt{-\ln\left(\frac{n^{\Omega}}{n_{max}}\right)}\right] \quad (21)$$

The differential energy of adsorption is obtained by differentiating Eq. (18) with respect to $T$ and $V$:

$$\Delta\bar{\mu}_a = \left(\frac{\partial \Delta U_a}{\partial n^{\Omega}}\right)_{T,V} = RT - \alpha\sqrt{-\ln\left(\frac{n^{\Omega}}{n_{max}}\right)} \quad (22)$$

The isosteric heat of adsorption of hydrogen, $\Delta\bar{h}_a$ then can be calculated from substituting Eq. (13) into Eq. (22) with:

$$\Delta\bar{h}_a = \Delta\bar{\mu}_a - RT = -\alpha\sqrt{-\ln\left(\frac{n^{\Omega}}{n_{max}}\right)} \quad (23)$$

It is now a function of absolute adsorption only. The differential energy of adsorption $\Delta\bar{\mu}_a$ and isosteric heat of adsorption $\Delta\bar{h}_a$ as function of loading is shown in Fig. 10. The value of isosteric heat of adsorption falls within the range of the published literatures, the comparison is made in Table 6. It decreases with the amount absorbed. At the limit of zero pressure, the differential energy and isosteric heat of adsorption are infinite. This singularity originates from D–A model which has no Henry's law limit [36]. The isosteric heat of adsorption of C1 is around 7 kJ/mol, which is consistent with a physisorption process.

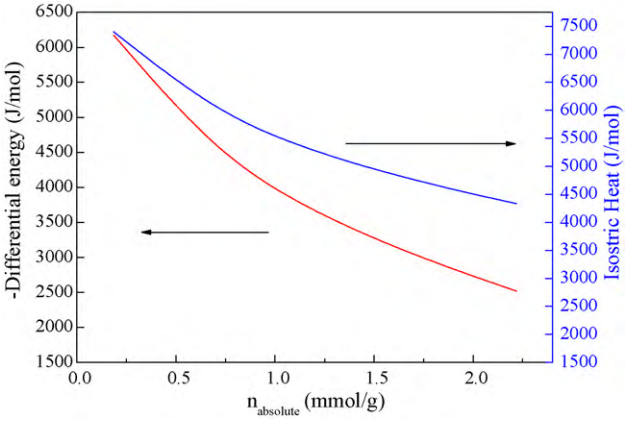


**Fig. 10.** Differential energy of adsorption and isosteric heat of adsorption as function of loading for C1 and hydrogen.

**Table 6**
Comparison of isosteric heat of adsorption of the carbon based material with hydrogen.

| Material | Isosteric heat of adsorption $\Delta\bar{h}_a$ (kJ/mol) | Reference |
|---|---|---|
| Activated carbon | 2–7 | [31] |
| Activated carbon | 5–6.5 | [33] |
| Activated carbon | 6–9 | [34] |
| Ordered mesoporous carbon MCM-48 | 6–8 | [35] |
| Ordered mesoporous carbon SBA-15 | 6–8 | [35] |
| C1 | 4–7 | This work |

## 4. Conclusions

Activated carbons were produced from corncob using different activation strategies and activators. Among them, the carbon produced by two-step KOH activation with the aid of ultrasonic treatment during the infiltration process yields the largest BET specific surface area and pore volume, which are 3012 $m^2/g$ and 1.7 $cm^3/g$, respectively. All carbons show microporous character, except for the sample that is activated by one-step phosphorous acid activation which shows hysteresis typical of mesoporous character. The FT-IR spectroscopy result indicates that the produced carbons are rich in surface functional groups. All the carbon show hydrogen adsorption capacity with C1 showing the largest capacity of 2.0 wt% at 77 K and 1 atm and 0.44 wt% at 298 K and 5 MPa, respectively. Carbon C5, which has a mesoporous character, shows the poorest performance in adsorbing hydrogen. This indicates the fact that hydrogen uptake at cryogenic conditions tends to correlates directly with the formation and development of micropores of the adsorbent. The isosteric heat of adsorption of C1 with hydrogen was approximately 7 kJ/mol, which is consistent with physisorption. Our research also indicates that preparation of activated carbon from corncob with super high specific surface area is a promising approach for high value conversion of abundant agricultural waste.

## Acknowledgements

Financial support for this work was provided by Monash University. The authors also want to thank the kind help of Dr. Kelvin Li, Dr. Gong-Kui Xiao, Dr. Liying Liu in the Adsorption Engineering Laboratory at Monash University.

## References

[1] L. Schlapbach, A. Zuttel, Hydrogen-storage materials for mobile applications, Nature 414 (2001) 353–358.
[2] U. Sahaym, M.G. Norton, Advances in the application of nanotechnology in enabling a 'hydrogen economy', J. Mater. Sci. 43 (2008) 5395–5429.
[3] D. Lozano-Castelló, M.A. Lillo-Ródenas, D. Cazorla-Amrós, A. Linares-Solano, Carbon 39 (2001) 741–749.
[4] Y.X. Yang, R.K. Singh, P.A. Webley, Hydrogen adsorption in transition metal carbon nano-structures, Adsorption 14 (2008) 265–274.
[5] Y. Sun, J.P. Zhang, G. Yang, Z.H. Li, An improved process for preparing activated carbon with large specific surface area from corncob, Chem. Biochem. Eng. Q. 21 (2007) 169–174.
[6] Y. Sun, J.P. Zhang, G. Yang, Z.H. Li, Removal of pollutants with activated carbon produced from $K_2CO_3$ activation of lignin from reed black liquors, Chem. Biochem. Eng. Q. 20 (2006) 429–435.
[7] K.L. John, J.J. Vijaya, G. Sekaran, Effect of two-stage process on the preparation and characterization of porous carbon composite from rice husk by phosphoric acid activation, Ind. Eng. Chem. Res. 43 (2004) 1832–1838.
[8] S.G. Badie, A.E. Abdel-Nasser, Porosity development in activated carbons obtained from date pits under chemical activation with phosphoric acid, Micropor. Mesopor. Mater. 52 (2002) 105–117.
[9] Z.X. Wu, Y.X. Yang, B. Tu, P.A. Webley, D.Y. Zhao, Adsorption of xylene isomers on ordered hexagonal mesoporous FDU-15 polymer and carbon materials, Adsorption 15 (2009) 123–132.
[10] B. Xiao, X.F. Sun, R.C. Sun, Chemical, structural, and thermal characterizations of alkali-soluble lignins and hemicelluloses, and cellulose from maize stems, rye straw, and rice straw, Polym. Degrad. Stabil. 74 (2001) 307–319.
[11] S.J. Gregg, S.W. Sing, Adsorption, Surface Area and Porosity, second ed., Academic Press, New York, 1982, pp. 195–228.
[12] R.L. Tseng, S.K. Tseng, F.C. Wu, Preparation of high surface area carbons from Corncob with KOH etching plus $CO_2$ gasification for the adsorption of dyes and phenols from water, Colloid Surf. A 279 (2006) 69–78.
[13] R.L. Tseng, S.K. Tseng, Pore structure and adsorption performance of the KOH-activated carbons prepared from corncob, J. Colloid Interface Sci. 287 (2005) 428–437.
[14] W.T. Tsai, C.Y. Chang, S.L. Lee, A Low cost adsorbent from agricultural waste corn cob by zinc chloride activation, Bioresour. Technol. 64 (1998) 211–217.
[15] D. Prahas, Y. Kartika, N. Indraswati, S. Ismadji, Activated carbon from jackfruit peel waste by $H_3PO_4$ chemical activation: pore structure and surface chemistry characterization, Chem. Eng. J. 140 (2008) 32–42.
[16] M.J. Prauchner, V.M.D. Vanya, N.D.S. Molhallem, C. Otani, S. Otani, L.C. Pardini, Structural evolution of Eucalyptus tar pitch-based carbons during carbonization, Biomass Bioenergy 28 (2005) 53–61.
[17] Y. Sun, J.P. Zhang, G. Yang, Z.H. Li, Study on the Corn stover Lignin oxidized by chlorine dioxide and reacted with furfuryl alcohol, Spectrosc. Spect. Anal. 27 (2007) 1997–2000.
[18] J. Jagiello, A. Ansón, M.T. Martínez, DFT-Based prediction of high-pressure $H_2$ adsorption on porous carbons at ambient temperatures from low-pressure adsorption data measured at 77 K, J. Phys. Chem. B 110 (2006) 4531–4534.
[19] A. Ansn, E. Lafuente, E. Urriolabeitia, R. Navarro, A.M. Benito, W.K. Maser, M.T. Martnez, Hydrogen capacity of palladium-loaded carbon materials, J. Phys. Chem. B 110 (2006) 6643–6648.
[20] C. Guan, X. Zhang, K. Wang, C. Yang, Investigation of $H_2$ storage in a templated carbon derived from zeolite Y and PFA, Sep. Purif. Technol. 66 (2009) 565–569.
[21] K.S. Xia, Q.M. Gao, C.D. Wu, S.Q. Song, M.L. Ruan, Activation, characterization and hydrogen storage properties of the mesoporous carbon CMK-3, Carbon 45 (2007) 1989–1996.
[22] J.X. Dong, G.Z. Ban, Q. Zhao, L. Liu, J.P. Li, Hydrogen storage in several metal-phosphate molecular sieves, AIChE J. 54 (2008) 3017–3025.
[23] M. Choi, R. Ryoo, Mesoporous carbons with KOH activated framework and their hydrogen adsorption, J. Mater. Chem. 17 (2007) 4204–4209.
[24] Z.X. Yang, Y.D. Xia, R. Mokaya, Enhanced hydrogen storage capacity of high surface area Zeolite-like carbon materials, J. Am. Chem. Soc. 129 (2007) 1673–1679.
[25] L. Zhou, Y.P. Zhou, A comprehensive model for the adsorption of supercritical hydrogen on activated carbon, Ind. Eng. Chem. Res. 35 (1996) 4166–4168.
[26] H.L. Wang, Q.M. Gao, J. Hu, High hydrogen storage capacity of porous carbons prepared by using activated carbon, J. Am. Chem. Soc. 131 (2009) 7016–7022.
[27] C.C. Huang, H.M. Chen, C.H. Chen, J.C. Huang, Effect of surface oxides on hydrogen storage of activated, Sep. Purif. Technol. 70 (2010) 291–295.
[28] Y.W. Li, R.T. Yang, Hydrogen storage in metal-organic frameworks by bridged hydrogen spillover, J. Am. Chem. Soc. 128 (2006) 8136–8137.
[29] A.L. Myers, Thermodynamics of adsorption in porous materials, AIChE J. 48 (2002) 145–160.
[30] A.L. Myers, P.A. Monson, Adsorption in porous materials at high pressure: theory and experiment, Langmuir 18 (2002) 10261–10273.
[31] M.A. Richard, P. Benard, R. Chahine, Gas adsorption process in activated carbon over a wide temperature range above the critical point. Part 2. Conversion of mass and energy, Adsorption 15 (2009) 53–63.
[32] M.A. Richard, P. Benard, R. Chahine, Gas adsorption process in activated carbon over a wide temperature range above the critical point. Part 1. Modified Dubinin-Astakhov model, Adsorption 15 (2009) 43–51.
[33] Y.P. Zhou, L. Zhou, Experimental study on high-pressure adsorption pf hydrogen on activated carbon, Sci. China 39 (1996) 598–607.
[34] Y.X. Yang, L. Bourgeois, C.X. Zhao, D.Y. Zhao, A. Chaffee, P.A. Webley, Ordered micro-porous carbon molecular sieves containing well-dispersed platinum nanoparticles for hydrogen storage, Micropor. Mesopor. Mater. 119 (2009) 39–46.
[35] T. Roussel, R.J.M. Pellenq, M. Bienfait, C. Vix-Guterl, R. Gadiou, F. Beguin, M. Johnson, Thermodynamic and neutron scattering study of hydrogen adsorption in two mesoporous ordered carbons, Langmuir 22 (2006) 4614–4619.
[36] D.M. Ruthven, Principles of Adsorption and Adsorption Processes, John Wiley & Sons, New York, 1984, pp. 1–100.